RESEARCH PAPER

PCCP
www.rsc.org/pccp

# Scanning electrochemical microscopy as a probe of $Ag^+$ binding kinetics at Langmuir phospholipid monolayers

**David P. Burt,[a] Javier Cervera,[ab] Daniel Mandler,[c] Julie V. Macpherson,[a] José A. Manzanares[d] and Patrick R. Unwin*[a]**

[a] *Department of Chemistry, University of Warwick, Coventry, UK CV4 7AL. E-mail: p.r.unwin@warwick.ac.uk*
[b] *Department of Experimental Sciences, Universitat Jaume I of Castellón, 12080 Castellón, Spain*
[c] *Department of Inorganic and Analytical Chemistry, Hebrew University of Jerusalem, Jerusalem, 91904, Israel*
[d] *Department of Thermodynamics, Faculty of Physics, University of Valencia, 46100 Burjassot, Spain*

***Received 11th May 2005, Accepted 7th June 2005***
***First published as an Advance Article on the web 30th June 2005***

A new method has been developed for measuring local adsorption rates of metal ions at interfaces based on scanning electrochemical microscopy (SECM). The technique is illustrated with the example of $Ag^+$ binding at Langmuir phospholipid monolayers formed at the water/air interface. Specifically, an inverted 25 μm diameter silver disc ultramicroelectrode (UME) was positioned in the subphase of a Langmuir trough, close to a dipalmitoyl phosphatidic acid (DPPA) monolayer, and used to generate $Ag^+$ *via* Ag electro-oxidation. The method involved measuring the transient current–time response at the UME when the electrode was switched to a potential to electrogenerate $Ag^+$. Since the $Ag^+$/Ag couple is reversible, the response is highly sensitive to local mass transfer of $Ag^+$ away from the electrode, which, in turn, is governed by the interaction of $Ag^+$ with the monolayer. The methodology has been used to determine the influence of surface pressure on the adsorption of $Ag^+$ ions at a phospholipid (dipalmitoyl phosphatidic acid) Langmuir monolayer. It is shown that the capacity for metal ion adsorption at the monolayer increased as the density of surface adsorption sites increased (by increasing the surface pressure). A model for mass transport and adsorption in this geometry has been developed to explain and characterise the adsorption process.

## Introduction

The process of metal ion binding at biomaterials (biosorption[1]) is of widespread importance and relevance. Notable examples include (trans-membrane) ion transport,[2] the extraction of toxic metals from industrial effluent,[3,4] precious metal reclamation[5] and trace metal analysis.[6,7] In cell biology, ion transfer regulates cellular processes[8] and the uptake of metal ions into cells has been shown to be partly due to energy-dependent transport, but also due to adsorption at particular functional groups.[9] The binding sites for metal ions at cell membrane surfaces are often quite specific,[10,11] with the carboxyl-terminating group representing an important component in the complexation of metal ions with cell membranes.[10–14]

The interaction of metal ions with phospholipid assemblies has been further exemplified through studies at Langmuir monolayers. Monolayers of phospholipids at the water/air (W/A) interface are increasingly recognised as sufficiently realistic models for cell membranes.[15–19] Studies conducted at acidic Langmuir monolayers at the W/A interface have shown the adsorption process to depend on the ion concentration,[20] monolayer composition[21] and subphase pH,[22] with trends similar to those found in studies of biological cells.

Adsorption at Langmuir monolayers has largely been deduced *via* physical changes in the monolayer structure, observed through the combination of techniques such as surface pressure measurements,[22,23] Brewster angle microscopy,[23] ellipsometry,[23] Fourier transform infrared spectroscopy,[22] atomic force microscopy,[24] Langmuir–Blodgett methods[25] and neutron activated analysis.[25] However, none of these studies have provided information on the local kinetics of ion adsorption. We have thus developed a technique to quantitatively determine metal ion uptake kinetics based on the use of ultramicroelectrodes (UMEs) and scanning electrochemical microscopy (SECM). Some of the unique features of UMEs[26–28] that make them suitable for measuring fast adsorption kinetics include high mass transport rates and fast response time that enables measurements to be made on the microsecond timescale (or shorter).[29,30]

In SECM, a UME is placed close to an interface of interest and used to either perturb and/or monitor a process of interest.[31–36] Previous investigations of phospholipid monolayers and related systems using SECM have included: induced desorption (SECMID[34]) processes;[37–39] induced transfer (SECMIT[40]), to measure passive trans-membrane diffusion;[41,42] double potential step chronoamperometry to investigate trans-membrane diffusion.[43,44] Several SECM techniques have also been employed to measure lateral diffusion in Langmuir monolayers.[38,45–47]

In the studies herein, we have applied the versatile nature of SECM[48] to study directly silver ion uptake kinetics and measure the resulting surface coverage at a molecular monolayer. Silver ion binding was of interest for three reasons. First, silver ions have previously been reported to have a high affinity for cell membranes, with maximum adsorption at pH values 5–6,[11,13] which is similar to the conditions employed for the studies herein. Second, from a technical viewpoint, silver microwires are readily available and compatible with the

DOI: 10.1039/b506611e

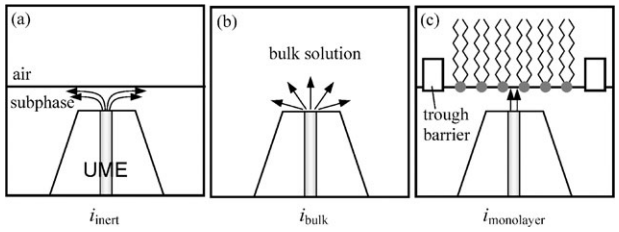


**Fig. 1** Schematic (not to scale) comparing diffusion of electrogenerated material ($Ag^+$) from an UME to: (a) an inert interface; (b) into bulk solution; (c) towards an interface where there is uptake of material. In the case shown, the clean W/A interface is inert (a) and hinders diffusion, resulting in a lower current ($i_{inert}$) to maintain the electrode surface concentration. In (b) $Ag^+$ ions diffuse hemispherically from the electrode surface and a current $i_{bulk}$ flows. In (c) the lipid monolayer adsorbs $Ag^+$ ions, so increasing the current with respect to case (a).

UME fabrication process. Third, the $Ag/Ag^+$ couple is extremely reversible and, as we demonstrate herein, this property allows any interaction of $Ag^+$ with a nearby interface to be determined directly from the current response of an Ag electrode undergoing anodic dissolution to form $Ag^+$.

The experimental approach reported in this paper is to position a silver UME probe close to the W/A interface (with a deposited monolayer) in the subphase of a Langmuir trough. The potential at the UME tip is stepped to a value where the silver electrode undergoes anodic dissolution, and electrogenerated $Ag^+$ diffuses away from the electrode vicinity, ultimately establishing a steady-state current. For an inert interface, $Ag^+$ diffusion is hindered by the interface. Thus, the current flow needed to maintain the $Ag^+$ concentration adjacent to the electrode surface, at the level dictated by the electrode potential of the reversible $Ag/Ag^+$ couple, is greatly diminished compared to the situation where the probe electrode is in bulk solution. This scenario is expected for a clean W/A interface (Fig. 1a). In bulk solution, without the influence of an interface, the generation of $Ag^+$ ions will ultimately form a hemispherical diffusion field (Fig. 1b) resulting in a current $i_{bulk}$. The current, $i_{bulk}$, will be greater than for the case of no uptake ($i_{inert}$) in Fig. 1a. In the case where $Ag^+$ ions bind to the monolayer (Fig. 1c) there will be an initial period of an enhanced flux of $Ag^+$ away from the UME towards the monolayer until the surface binding sites become saturated. At this point, the monolayer will become inert to further uptake and so there will be a switch to the behaviour for an inert interface. As we show in this paper through experiment and theory, the distinct current–time characteristics for these different cases are diagnostic of the rate and extent of $Ag^+$ binding at the interface.

## Theory

The theoretical model for the SECM response is based on a Langmuirian adsorption process for $Ag^+$ binding at the monolayer. It is assumed that only $Ag^+$ ions generated at the electrode adsorb at the monolayer. This assumption is justified since the $TMA^+$ cation, used as the subphase supporting electrolyte, has only a weak binding affinity for the phospholipid.[46]

A schematic (not to scale) of the simulation domain for the adsorption of $Ag^+$ ions, generated at a silver UME close to a monolayer, is shown in Fig. 2. In the presence of an excess of supporting electrolyte, the transport of $Ag^+$ ions in the solution can be described as a time-dependent diffusion process. The equation to be solved appropriate to the axisymmetric cylindrical geometry of SECM is:

$$\frac{\partial c}{\partial t} = D\left(\frac{\partial^2 c}{\partial r^2} + \frac{1}{r}\frac{\partial c}{\partial r} + \frac{\partial^2 c}{\partial z^2}\right) \qquad (1)$$

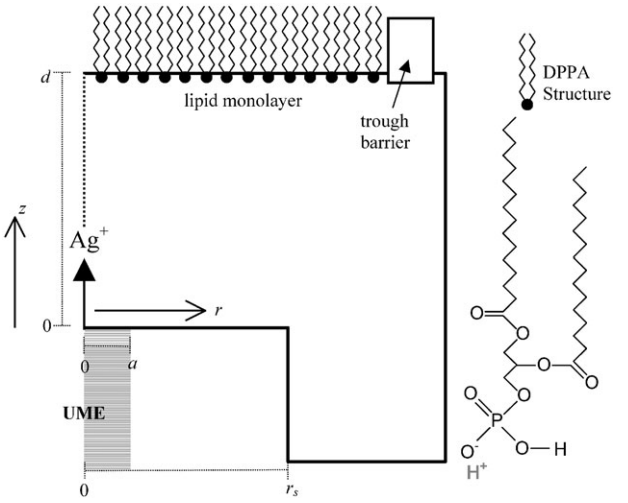


**Fig. 2** SECM axis-symmetric cylindrical geometry and coordinate system used for the simulations, together with the schematic of dipalmitoyl phosphatidic acid (DPPA).

where $c$ and $D$ are the concentration and diffusion coefficient of the $Ag^+$ ions, respectively, $r$ and $z$ are the radial and normal directions relative to the electrode starting at its centre, and $t$ is time.

Initially no $Ag^+$ ions are present in solution, therefore we can write

$$t = 0, 0 \le r \le r_s,\ 0 \le z \le d\text{: } c = 0 \qquad (2)$$

where $r_s$ is the radius of the insulating glass sheath and $d$ is the distance between the electrode surface and the monolayer interface. Since the generation of $Ag^+$ is reversible at the electrode, the boundary conditions at the electrode surface is:

$$0 \le r \le a,\ z = 0,\ t > 0\text{: } c = c_s \qquad (3)$$

where $c_s$ is the concentration of $Ag^+$ ions at the electrode surface and $a$ is the electrode radius.

Since the insulating glass around the electrode is considered inert to the $Ag^+$ ions,

$$a < r \le r_s,\ z = 0,\ t > 0 : D\left(\frac{\partial c}{\partial z}\right) = 0 \qquad (4)$$

Further boundary conditions are the null radial flux at the axis of cylindrical symmetry

$$r = 0,\ 0 \le z \le d,\ t > 0 : D\left(\frac{\partial c}{\partial r}\right) = 0 \qquad (5)$$

and the assumption that no $Ag^+$ ions will reach the edge of the insulating glass of the electrode during the experiment,

$$r = r_s,\ 0 \le z \le d,\ t > 0\text{: } c = 0 \qquad (6)$$

This is a reasonable assumption considering the time interval of the experiment and that $r_s \approx 10a$. The boundary condition at the monolayer is controlled by the binding of $Ag^+$ ions

$$\alpha N \frac{\partial \theta}{\partial t} = k_a c(1 - \theta) \qquad (7)$$

$$0 \le r \le r_s,\ z = d,\ t > 0 : D\frac{\partial c}{\partial z} = k_a c(1 - \theta) \qquad (8)$$

where $N$ is the surface density of the phospholipids of the monolayer, of which a fraction $\alpha$ is deprotonated, $\theta$ is the fraction of deprotonated phospholipids with bound $Ag^+$ ions, and $k_a$ is the kinetic rate constant for the binding process. This formulation of the kinetic problem assumes that binding occurs exclusively at anionic sites, which is reasonable, in light of the results that follow. The adsorption process is treated as

irreversible (no desorption), since we are interested in the initial capture of $Ag^+$ ions at the monolayer. The high excess of $Ag^+$ generated by the UME ensures that a flux of $Ag^+$ ions is directed towards the monolayer to drive the binding process.

The value of $k_a$ is usually considered to be constant if the adsorption process follows simple Langmuir kinetics. However, since the interface is initially negatively charged and the $Ag^+$ binding neutralises the charge, the value of $k_a$ may depend on the electric potential at the monolayer $\psi_0$ (with respect to the bulk solution) through

$$k_a = k_a^i \exp(-F\psi_0/2RT) \tag{9}$$

where $F$ is the Faraday constant, $R$ is the gas constant and $T$ is the temperature of the system and $k_a^i$ is an intrinsic rate constant. Here, the charge density ($\sigma$), $\psi_0$ relationship of the monolayer is assumed to follow the Gouy–Chapman model,[37,49]

$$\sigma = (8\varepsilon\varepsilon_0 RTI)^{1/2} \sinh(F\psi_0/2RT) \leq 0 \tag{10}$$

where $\varepsilon$ and $\varepsilon_0$ are the relative dielectric permittivity and the dielectric permittivity of the vacuum, respectively, and $I$ is the ionic strength of the solution, which is assumed to be set by the supporting electrolyte. We provide a fuller consideration of some of the issues involved in this formulation in the Appendix and justify the approach taken.

The value of the surface charge density at the monolayer depends on the surface density of deprotonated phospholipids, $\alpha N$, and on the fraction $\theta$ of $Ag^+$ bound

$$\sigma = \alpha NF(\theta - 1) \leq 0 \tag{11}$$

Eqns. (1) to (8) form the system of equations with their boundary conditions that we need to solve for the simplest case, with the addition of eqns. (9) to (11) if the adsorption process is considered potential-dependent. This system was solved numerically using the Finite Element Method for the spatial variables and a 'stiff' Runge–Kutta method for the time-dependence. The commercial package Femlab®, and extension of Matlab® were used to this effect. For the simplest case (potential independent rate constant), the problem was also solved using the alternating direction implicit finite difference method,[37] with identical results to the finite element simulation.

Before proceeding to the numerical simulation of the system, the equations were cast into dimensionless form using the variables

$$\tau \equiv \frac{D}{a^2}t;\ R \equiv \frac{r}{a};\ Z \equiv \frac{z}{a} \tag{12}$$

$$C \equiv \frac{c}{c_s};\ \phi \equiv \frac{\alpha N}{ac_s};\ K_a \equiv \frac{k_a a}{D} \tag{13}$$

The diffusion equation then takes the form

$$\frac{\partial C}{\partial \tau} = \frac{\partial^2 C}{\partial R^2} + \frac{1}{R}\frac{\partial C}{\partial R} + \frac{\partial^2 C}{\partial Z^2} \tag{14}$$

and the initial condition is

$$\tau = 0,\ 0 \leq R \leq R_s,\ 0 \leq Z \leq L\text{: } C = 0 \tag{15}$$

where $R_s \equiv r_s/a$ and $L \equiv d/a$, and the following boundary conditions apply

$$0 \leq R \leq 1,\ Z = 0,\ \tau > 0\text{: } C = 1 \tag{16}$$

$$1 < R \leq R_s,\ Z = 0,\ \tau > 0\text{: } \frac{\partial C}{\partial Z} = 0 \tag{17}$$

$$R = 0,\ 0 \leq Z \leq L,\ \tau > 0\text{: } \frac{\partial C}{\partial R} = 0 \tag{18}$$

$$R = R_s,\ 0 \leq Z \leq L,\ \tau > 0\text{: } C = 0 \tag{19}$$

$$0 \leq R \leq R_s,\ Z = L,\ \tau > 0\text{: } \frac{\partial C}{\partial Z} = K_a C(1 - \theta) \tag{20}$$

The time-dependence of $\theta$ is given by:

$$\phi\frac{\partial \theta}{\partial \tau} = K_a C(1 - \theta) \tag{21}$$

with the following initial condition:

$$\tau = 0,\ 0 \leq R \leq R_s\text{: } \theta = 0 \tag{22}$$

The experimental method involved recording and analysing the current–time behaviour of the UME probe, following the potential step to electrogenerate $Ag^+$. Consequently, the normalised current at the electrode was calculated:

$$\frac{i}{i_\infty} = \frac{\pi}{2}\int_0^1 r\left.\frac{\partial C}{\partial Z}\right|_{Z=0} \mathrm{d}r \tag{23}$$

where

$$i_\infty = 4nFaDc_s \tag{24}$$

is the steady-state current at a disk electrode for a $n$-electron transfer process ($n = 1$ for the anodic dissolution of Ag forming $Ag^+$).

## Theoretical results and discussion

For the simplest case, where the adsorption rate constant is not potential dependent, the UME current–time behaviour depends on the distance between the electrode and the monolayer, $L$, the kinetic rate constant, $K_a$, and the fractional surface concentration of deprotonated phospholipid, $\phi$. Fig. 3 shows the normalised current as a function of (normalised) time for $K_a = 5$ and $\phi = 0.1$, and different values of the distance ($L$ = 0.24, 0.32, 0.40, 0.48). The rate constant represents a moderate value, where an effect of the adsorption on the UME response is seen, but the process is well below the diffusion limit. For a typical value of $a$ = 12.5 μm and $c_s = 10^{-6}$ mol $cm^{-3}$, the value $\phi = 0.1$ represents a surface site density of about $1.25 \times 10^{-10}$ mol $cm^{-2}$. In the initial time interval, before the electrogenerated $Ag^+$ ions reach the monolayer, the current values for all cases are equal because the behaviour is simply governed by the diffusion of $Ag^+$ away from the electrode over a short distance compared to the tip to monolayer separation (predominantly planar diffusion on this timescale). Once $Ag^+$ ions reach the monolayer the different cases deviate from one another, on a timescale governed by the tip to monolayer diffusion time, which is of the order of the square of the normalised distance, $L^2$. The interaction of the $Ag^+$ ions

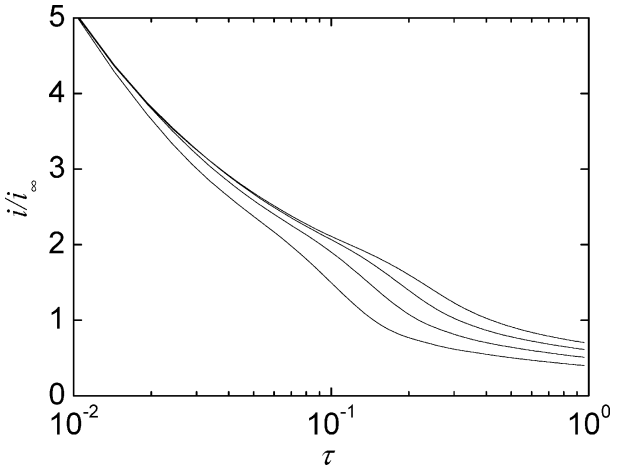


**Fig. 3** Normalised current as a function of normalised time for $K_a = 5$, $\phi = 0.1$, for dimensionless distances $L$ (from bottom to top) 0.24, 0.32, 0.40, and 0.48.

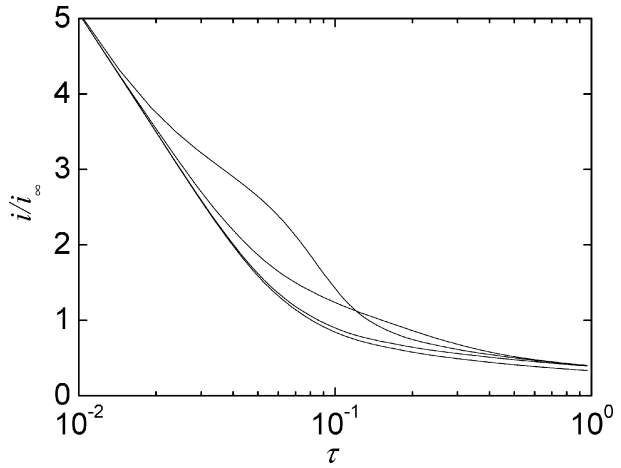


**Fig. 4** Normalised current as a function of normalised time for $L = 0.24$, $\phi = 0.1$, and the dimensionless kinetic rate constants $K_a$ (from bottom to top) 0.01, 0.1, 1, and 10.

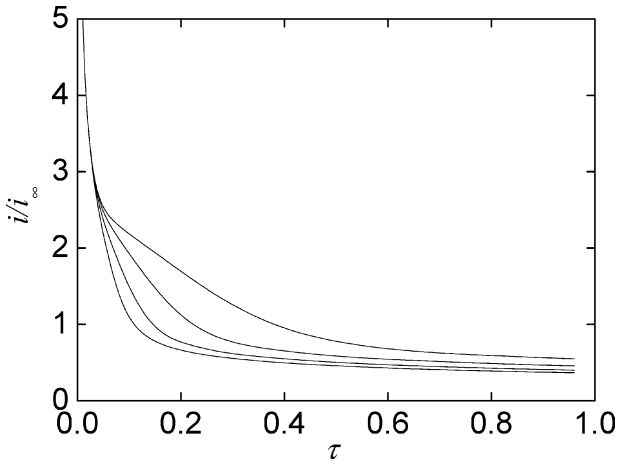


**Fig. 5** Normalised current as a function of normalised time for $L = 0.24$, $K_a = 5$, and the dimensionless surface concentration of phospholipids $\phi$ (from bottom to top) 0.05, 0.1, 0.2, and 0.4.

with the monolayer serves to enhance the flux of $Ag^+$ away from the electrode compared to the case where there is no interaction (clean air/water interface), so increasing the current compared to this inert interface limiting case.

As the monolayer tends towards saturation, the rate of the adsorption process decreases and this is reflected in a decrease in the current with time towards the behaviour for an inert interface. Clearly, the shorter the tip to monolayer diffusion time (closer the distance), the earlier is this limiting case reached. As in previous studies of interfacial kinetics with SECM,[31] the data in Fig. 3 demonstrate that the current response of the probe electrode becomes most sensitive to the interfacial process as the tip-surface distance is decreased. Since the density of surface sites could be an order of magnitude higher than considered here for some systems, the data in Fig. 3 highlight the sensitivity of the method to adsorption processes.

Fig. 4 shows effect of the rate constant, $K_a$, on the normalised current–time behaviour for $\phi = 0.1$ at a dimensionless distance, $L = 0.24$ (which corresponds to a typical distance of 3 μm in the experiments reported later, with $a = 12.5$ μm). As for the data in Fig. 3, the initial current–time behaviour is essentially Cottrellian for all cases, until a time is reached when the diffusion field propagating from the probe electrode intercepts the monolayer. Thereafter, the current–time response depends on $K_a$. In the initial period, beyond $\tau \approx 0.015$, the larger the rate constant, the higher is the current since there is an increased flux of $Ag^+$ away from the electrode as a consequence of the faster adsorption process. However, since the uptake of $Ag^+$ by the monolayer also depends on the fraction of the available sites, $1 - \theta$, as the region of the monolayer directly opposite the electrode tends to saturation, that part of the interface begins to behave as an inert substrate, and so the current value decreases. The larger the value of $K_a$, the faster is the filling of the binding sites of the monolayer and so the earlier the tendency towards the behaviour for an inert interface. Thus, a time can be reached where the current for the case with a larger rate constant may become smaller than that for a system with a smaller rate constant. This can be seen in Fig. 4, where the current for the highest value of $K_a = 10$ crosses the current for $K_a = 1$ at $\tau \approx 0.11$. As further time elapses saturation of the monolayer binding sites is achieved in all cases and they tend, asymptotically, to behave like the system with an inert substrate.

The dependence of the system, with respect to the surface density of adsorption sites, or electrode-surface concentration of $Ag^+$, is shown in Fig. 5. This presents the normalised current, as a function of normalised time, for different values of the parameter $\phi$, for $L = 0.24$ and $K_a = 5$. When $c_s$ and $a$ are constant, $\phi$ represents the initial concentration of surface adsorption sites (eqn. (13)). It can clearly be seen that the rate of uptake of $Ag^+$ by the monolayer, and thus the normalised current, increases with $\phi$. A longer period is also required for the monolayer to reach the saturation point the larger the value of $\phi$.

Since the current–time behaviour depends on how the surface binding sites are filled with time, it is informative to examine the $\theta$–$R$–$\tau$ relation for different values of $K_a$. The fraction of $Ag^+$ bound to the monolayer, $\theta$, is shown in Fig. 6 for normalised times 0.25, 0.50, 0.75, and 1.00, for $\phi = 0.1$ and $L = 0.24$ with: (a) $K_a = 0.01$; (b) $K_a = 10$. These data show the significant effect of the kinetic rate constant $K_a$ (note the different scale for $\theta$ in (a) and (b)). The adsorption process initially occurs predominantly in the region of the monolayer directly opposite the electrode and of similar size to the electrode radius until the saturation state, $\theta = 1$, is reached. Beyond this point, the adsorption region begins to widen with time, as can be seen in Fig. 6(b). As sites are filled on the surface further from the electrode, the concentration gradient at the electrode becomes less steep, thus explaining the decrease in current that is seen at medium to long times in current–time transients, such as those in Figs. 4 and 5. The data in Fig. 6 also indicate that the adsorption process can be localised by the SECM method by judicious selection of the timescale of the experiment.

To highlight the effect that the monolayer surface potential may have on the adsorption process, Fig. 7 shows the normalised current as a function of normalised time, considering a simple process of $K_a = 5$ (solid lines) and a potential-dependent process with the value of $K_a^1$ chosen so that $K_a = 5$ when $\theta = 0$ (dotted lines), *i.e.*, initially both curves correspond to the same value of the rate constant. The values of the constant parameters used in the latter case were $T = 300$ K, $I = 0.05$ M, and $\varepsilon = 80$ (set to the value for pure water). The distance was set to $L = 0.24$ and the cases of $\phi = 0.1$ (bottom lines) and $\phi = 0.4$ (top lines) are considered. The surface density of deprotonated

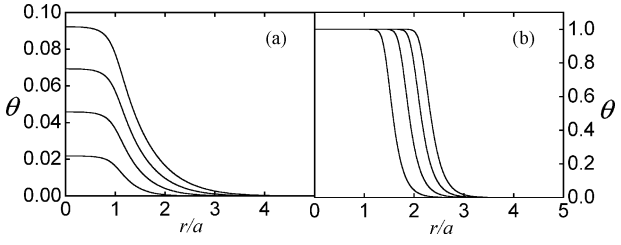


**Fig. 6** Fractional surface coverage of $Ag^+$ at a target interface as a function of $r/a$ for normalised times (from left to right) of 0.25, 0.50, 0.75 and 1.00. Simulations were run with $L = 0.24$, $\phi = 0.1$, and $K_a = 0.01$ (a) and $K_a = 10$ (b). (Note the difference in the scale.)

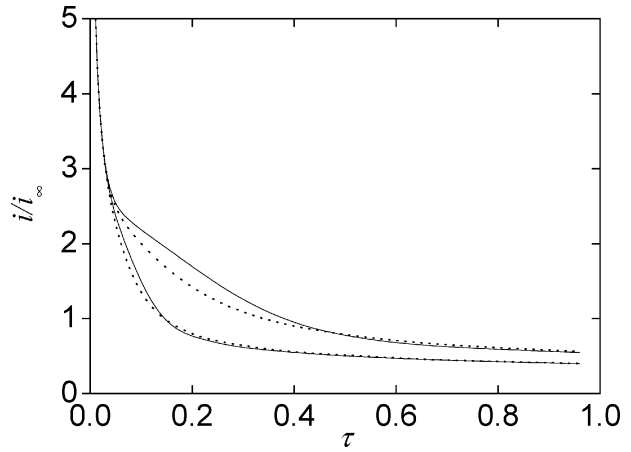


**Fig. 7** Normalised current as a function of normalised time for a simple (potential-independent) adsorption process with $K_a = 5$ (solid line) and a potential-dependent process with $K_a = 5$ when $\theta = 0$ (dotted line), for $L = 0.24$ and two values of $\phi$: 0.1 (bottom lines) and 0.4 (top lines).

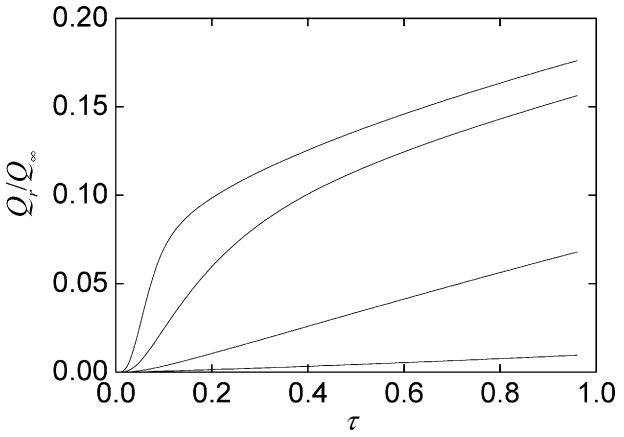


**Fig. 8** Normalised charge difference between a system with and without a monolayer generated at the electrode as a function of normalised time for $L = 0.24$, $\phi = 0.1$, and the dimensionless kinetic rate constants $K_a$ (from bottom to top) 0.01, 0.1, 1, and 10.

sites $\alpha N$ has been estimated as $\phi a c_s$ with $a = 12.5$ μm and $c_s = 10^{-6}$ mol cm$^{-3}$. Initially, the current for both cases is the same, but as $Ag^+$ ions bind to the monolayer, the negative charge is neutralised and so the rate constant for the potential-dependent process decreases (see eqns. (9)–(11)). This explains the lower current of this process, once it deviates from the potential-independent case. As for the effect of $K_a$ in the potential-independent process (see above, especially Fig. 4), a higher value of the rate constant leads to a faster saturation of the monolayer with $Ag^+$ ions. Thus, when comparing the potential-dependent and potential-independent cases, a time is reached where the current for the latter is lower than for the potential-dependent process (which is slower at intermediate times).

It is also evident from Fig. 7 that the extent to which the current–time characteristics for the two models are different depends largely on the value of $\alpha N$, which, in turn, governs the potential of the monolayer. For relatively low $\alpha N$, it is clear that the effect of surface charge on the current–time behaviour is a minor consideration.

Previous SECM studies of adsorption–desorption processes have involved the analysis of raw current–time data.[37,38] However, the current signal is convoluted by both the adsorption process and diffusion in solution. To essentially remove diffusional contributions, we suggest that the difference between the total charge generated at the electrode when adsorption occurs compared to a clean W/A interface, $Q_r$ is considered. Theoretically, this magnitude can be obtained by integrating the values of the current difference between the case with a monolayer, $i_{monolayer}$, and that with a clean W/A interface, $i_{clean}$

$$Q_r(t) = \int_0^1 dt' [i_{monolayer}(t') - i_{clean}(t')] \qquad (25)$$

Since the calculation of $Q_r$ implies integration with time, the treatment of data in this way will also be advantageous in eliminating some of the noise in experimental transients, as the noise will partially cancel, with the addition of the current values at the different times. To determine the sensitivity of $Q_r$ with respect to the parameters of the system, Figs. 8 and 9 show the dependence of the normalised charge difference $Q_r/Q_\infty$, where $Q_\infty \equiv (a^2/D)i_\infty$, with $K_a$ and $\phi$, respectively. The dependence of the generated charge difference with respect to $K_a$ can be seen in Fig. 8, where the values of $Q_r/Q_\infty$ as a function of normalised time are shown for $L = 0.24$ and $\phi = 0.1$, for several values of the dimensionless rate constant, $K_a$. Note that the values of $Q_r/Q_\infty$ do not cross, with respect to time, for the two higher constants as they did for the normalised current *versus* time (see Fig. 4). It can be seen that the difference in generated charge is very sensitive to the rate constant when the system is far from the diffusion-limit region ($K_a$ is small), but that some of this sensitivity is lost as the diffusion-limit is approached by the system. Finally, Fig. 9 shows the values of $Q_r/Q_\infty$ as a function of normalised time for $L = 0.24$, $K_a = 5$, and different values of $\phi$. It can be seen that the quantity $Q_r/Q_\infty$ *versus* time is particularly sensitive to the value of $\phi$.

## Experimental section

### Materials

Tetramethylammonium nitrate ($TMANO_3$, ≥ 98%) was purchased from Alfa Aesar. L-α-phosphatidic acid dipalmitoyl (DPPA, ≥ 99%) was acquired from Sigma-Aldrich. Methanol (AnalaR ≥ 99.8%) and chloroform (HiPerSolv for HPLC ≥ 99.8%) were purchased from BDH. All chemicals were used as received and aqueous solutions were prepared using purified Milli Q (Millipore Corp.) reagent water, which had a resistivity ≥ 18 MΩ cm.

### Apparatus and instrumentation

All electrochemical measurements were carried out in a Langmuir trough (Model 611, Nima Technology, Coventry, UK) shielded within a Faraday cage at ambient temperature (22 ±

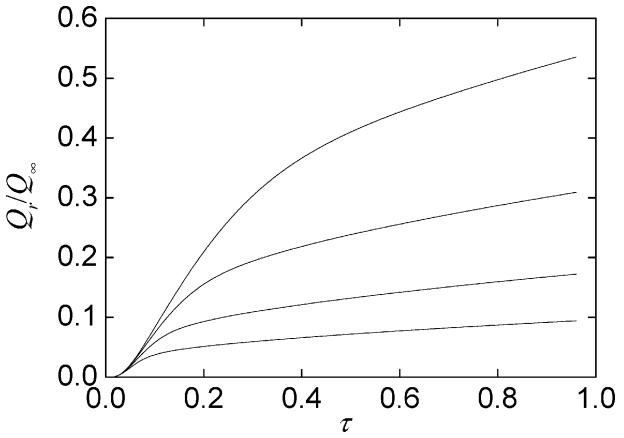


**Fig. 9** Normalised charge difference between the electrode response for a system with and without adsorption as function of normalised time for $L = 0.24$ and $K_a = 5$. Dimensionless surface concentrations are considered of $\phi$ (from bottom to top) 0.05, 0.1, 0.2, and 0.4.

1 °C) in an air conditioned room. The submarine UME tip was a 25 μm diameter Ag disc prepared according to a procedure described previously.[40,50] The UME tip geometry was characterised by a ratio $r_s/a = 10$ (ratio of the diameter of the surrounding insulating sheath to that of the electrode).[51] The submarine electrode was positioned using a set of $x,y,z$ stages (M-462, Newport Corp., CA) and a piezoelectric $z$-positioner and controller (Models P843.30 and E662, Physik Instrumente, Waldbronn, Germany). The inverted UME was positioned with respect to the W/A interface, using a holder comprised of a glass capillary tube inserted into a Teflon block (Fig. 10). Current–voltage curves and chronoamperometric data were acquired using a bipotentiostat fitted with a low current module (CH instruments, Model 730A, Austin, TX).

### Procedures

**Langmuir trough and subphase preparation.** The trough was cleaned using a lint-free tissue saturated with chloroform and then rinsed thoroughly with water. The W/A interface was swept clean by closing the barriers of the trough and contaminants were removed using a water vacuum pump. This procedure was repeated until no rise in surface pressure occurred during the compression stage. $TMANO_3$ was dissolved in purified water to serve as a 0.05 M subphase and background electrolyte. The pH of the subphase was recorded prior to the experiment.

**$Ag^+$ ion generation and electrochemical measurements.** Currents were measured in a two-electrode system at a 25 μm diameter silver disc submarine UME, with a chloridised silver wire acting as a reference electrode. For the generation of silver ions, a potential step was used to induce the anodic dissolution of the silver electrode and the resulting current was measured. The potential of the electrode was initially held at −0.20 V, where no faradaic processes occurred, for 10 s prior to the potential step. The current was monitored after the potential was stepped to 0.16 V, typically for a time period of 0.25 s. Current values were recorded every 0.0005 s, for the transient duration.

**Distance calibration.** As highlighted in 'Theoretical results and discussion', the distance between the UME and interface is a key variable that needs to be known if kinetic parameters are to be derived from experimental current–time transients. The induced transfer of $O_2$ across a clean W/A interface using SECM, has been demonstrated to be an effective technique when determining the distance between an UME and the W/A interface.[40] However, the presence of a compressed monolayer retards oxygen transfer across the W/A interface in a manner that is highly sensitive to surface pressure.[40] In a previous study we observed that the presence of a DPPA monolayer at the interface hindered the transfer of $O_2$ as reflected in the current response.[41] We also found that if oxygen reduction measurements were made at the UME, then subsequent silver anodic dissolution transients showed a non-ideal response, as evident from behaviour recorded with the probe positioned in bulk solution and against a clean W/A interface. We tentatively attribute this to the formation of a silver oxide on the electrode surface, brought about by the basic conditions ($\approx$pH 11).[52]

To avoid the above complications, the distance from the interface was determined using the normalised long-time limiting current measured by chronoamperometric transients, which was then fitted to the theoretical response for the generation of $Ag^+$ ions at an inert interface. This is reasonable, based on the theoretical results presented above, which showed that monolayer sites will become saturated at long times.

The UME was initially positioned in bulk solution and the transient current response for $Ag^+$ ion generation was measured. The electrode was then brought towards a clean W/A interface in a step-wise fashion (step size $\approx$ 10 μm) using a micrometer, with a transient for Ag anodic dissolution measured at each distance, until a change from the bulk response was measured. From this point, the UME was moved more accurately using the piezoelectric positioner (step size $\approx$ 0.5 μm). A wait time ($\approx$1 min) between transients was employed to allow the diffusion of $Ag^+$ ions away from the electrode-interface region. After recording a series of transients at numerous distances from the interface, the UME was retracted to bulk solution to allow for the lipid monolayer to be spread at the interface.

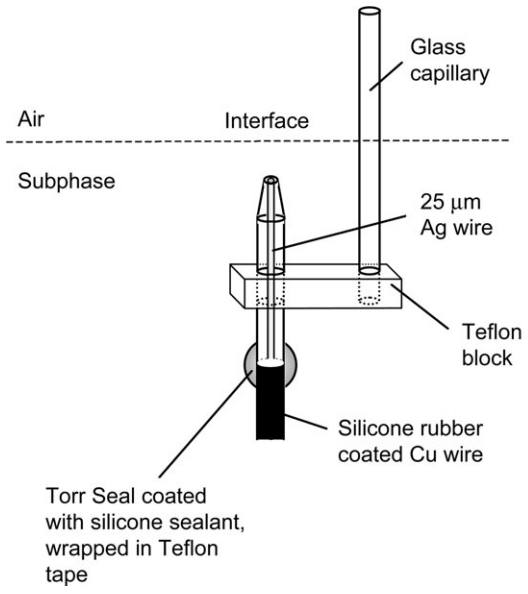


**Fig. 10** Schematic of a submarine Ag UME and holder positioned adjacent to the W/A interface.

**Langmuir film preparation.** A known volume (70 μl) of a 0.9 mg $ml^{-1}$ DPPA spreading solution, made from a 1 : 4 (v/v) methanol : chloroform solvent, was evenly presented to the subphase using a microsyringe (100 μl volume, Hamilton, Reno, NV). DPPA solutions were prepared on the day of use and stored at $<0$ °C. The spreading solvent was allowed to evaporate for 20 min prior to monolayer compression. Pressure–area isotherms were obtained by compressing the monolayer at a continuous speed of 25 $cm^2$ $min^{-1}$, whilst monitoring the surface pressure using a Wilhelmy plate.

**$Ag^+$ generation at the Langmuir film.** For SECM measurements the monolayer was held at pressures of 10, 20 and 30 mN $m^{-1}$. At each pressure, the UME was brought towards the monolayer in the same step-wise method used at the clean W/A interface. However, it is important to mention that between each $Ag^+$ generating transient, the electrode was translated laterally ($\approx$3 mm) to a different region of the Langmuir film. This was done to eliminate any possible effects due to transients made previously at the lipid monolayer. In addition, care was taken to avoid contacting the lipid monolayer with the UME, which was observed to cause electrode blocking. This could be avoided by monitoring the current recorded at long times, when adsorption sites are saturated and the monolayer behaves as an inert interface.

## Experimental results and discussion

### $Ag^+$ generation transients at an inert interface

The method proposed required that the current–time response for $Ag^+$ electrogeneration was well-defined and characterised.

 

Initial current–time curves for the anodic dissolution of the Ag UME were thus recorded with the electrode positioned at different distances from a clean W/A interface. In comparing experiment with the theoretical simulations, the following constants were used: $D = 1.5 \times 10^{-5}$ cm$^2$ s$^{-1}$, $a = 12.5$ μm, and $r_s = 10a$.

Fig. 11 shows typical experimental transients and theoretical fits to the curves, assuming simple hindered diffusion at an inert interface (*i.e.* strictly the model outlined herein with a no-flux boundary condition at the substrate, or eqn. (20) with $K_a = 0$). The top curve corresponds to the bulk solution while the bottom one corresponds to the smallest distance between the electrode and the interface. The steady-state current in the bulk solution, $i_\infty$ was the only unknown involved in fitting the bulk solution current–time transient, and for the case in Fig. 11 this was $i_\infty = 6.5$ nA. From this value the $Ag^+$ concentration at the electrode was obtained from eqn. (24), $c_s = 0.9$ mM. With $c_s$ fixed, the distance between the surface of the probe electrode and the clean interface was used as the fitting parameter for the rest of the measurements. The precise distances used can be found in the caption to Fig. 11, which identifies a closest distance of 3.0 μm between the electrode and the interface. The fit between experiment and theory is highly satisfactory over most of the timescale of the measurements. At the shortest times, the experimental current is consistently higher than predicted from the model, and this is attributed in the main to charging effects. This discrepancy is accounted for reasonably in the experimental analysis which follows, since the approach utilised relies on current-difference plots obtained from transients at the same distance with and without a monolayer present, to obtain the adsorption charge, $Q_r$ as outlined in 'Theory'. Thus, the current due to background processes in each case is effectively eliminated. Nonetheless, it is important to note that there is excellent agreement between experiment and theory on a timescale of a few ms and longer in Fig. 11.

### Pressure–area isotherm for a DPPA monolayer

A typical isotherm for a DPPA monolayer is shown in Fig. 12, from which it is clear that for molecular areas greater than 85 Å$^2$ per molecule the surface pressure is close to zero. As the area becomes smaller, there is first a transition from a liquid-expanded to liquid-condensed phase, based on previous similar

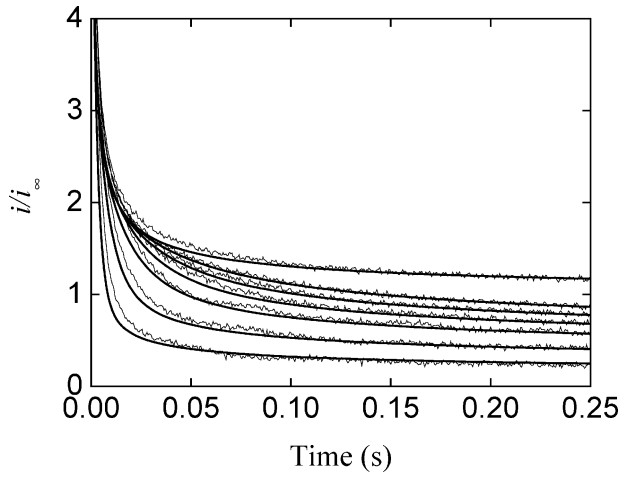


**Fig. 11** Measured normalised current as a function of time for the anodic dissolution of an Ag UME positioned at different distances from a clean W/A interface. The current steady-state current, $i_\infty = 6.5$ nA was derived from the bulk transient response (top curve). The fitting of the remaining transients used the distance $d$ as the only variable, with best fits obtained for (from bottom to top) 3 μm, 5 μm, 7.5 μm, 9 μm, 11 μm, and 13 μm. In all cases, theory is represented by the solid smooth curves.

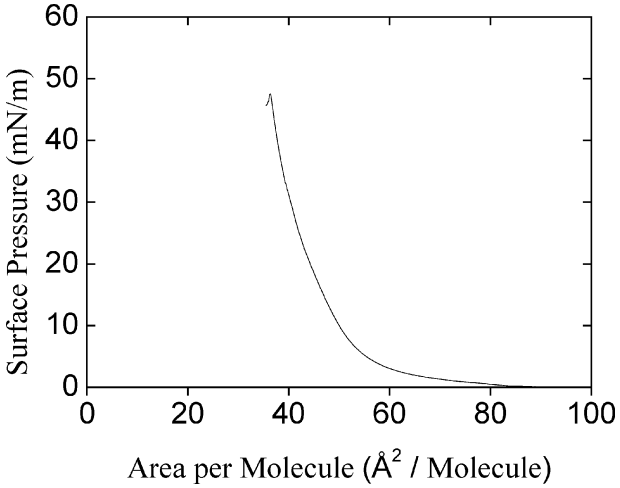


**Fig. 12** Pressure–area isotherm of dipalmitoyl phosphatidic acid (DPPA) spread on a 0.05 M tetramethylammonium nitrate aqueous subphase at pH 6.

deductions on a pH 6 water subphase at 25 °C.[53] Further compression brings the DPPA molecules closer together, causing the pressure to rise up to a collapse pressure of 47.5 mN m$^{-1}$, which is reasonably close to values reported for a DPPA monolayer on pure water (53 mN m$^{-1}$).[53] The limiting molecular area at the collapse pressure is obtained by extrapolation of the isotherm to zero pressure and was determined as 44 Å$^2$ per molecule, which is close to previously reported values for DPPA on pure water at pH 6 (42 ± 2 Å$^2$ per molecule).[54]

The pressure–area isotherm was used to estimate the surface site density, $N$, for the SECM measurements. The area per molecule at surface pressures of 10, 20, and 30 mN m$^{-1}$, used for the SECM experiments are 50, 44, and 40 Å$^2$ per molecule, respectively, and the corresponding values of $N$ are $3.3 \times 10^{-10}$, $3.8 \times 10^{-10}$, and $4.2 \times 10^{-10}$ mol cm$^{-2}$.

### $Ag^+$ generation transients at a DPPA monolayer

Measurements were made at the closest possible distance (3 μm) from the DPPA monolayer, to ensure that the SECM technique operated with greatest sensitivity. Fig. 13 shows typical transients, presented as normalised current (with $i_\infty = 6.5$ nA) as a function of time for a DPPA monolayer at surface pressures of 10 mN m$^{-1}$, 20 mN m$^{-1}$ and 30 mN m$^{-1}$. The behaviour for a clean W/A interface is also shown for comparison. It can clearly be seen that at the shortest times (up to *ca.* 2 ms) the currents recorded in each of the transients coincide. This is because on this timescale the diffusion field from the tip electrode does not reach the interface, and so the latter has no effect on the response. Thereafter, for times up to about 30 ms, the current with the monolayer present, at all of the pressures considered, is higher than for the clean W/A interface. The enhanced current with the lipid monolayer can be attributed to $Ag^+$ uptake at the monolayer. At times beyond *ca.* 30 ms, the behaviour tends towards the response based on hindered diffusion (clean W/A transient), which can be attributed to the adsorption sites tending to saturation. The excellent agreement between all of the transients at long times indicates that they were recorded at essentially the same tip–interface separation.

To obtain quantitative information on the adsorption process, we consider the analysis of data in terms of the quantity $Q_r$, which is the accumulated charge difference between transients recorded with and without a monolayer present. The data from Fig. 13, for the three surface pressures are presented in this manner in Fig. 14, using the clean W/A interface transient in Fig. 13 as the reference signal. The data in Fig. 14

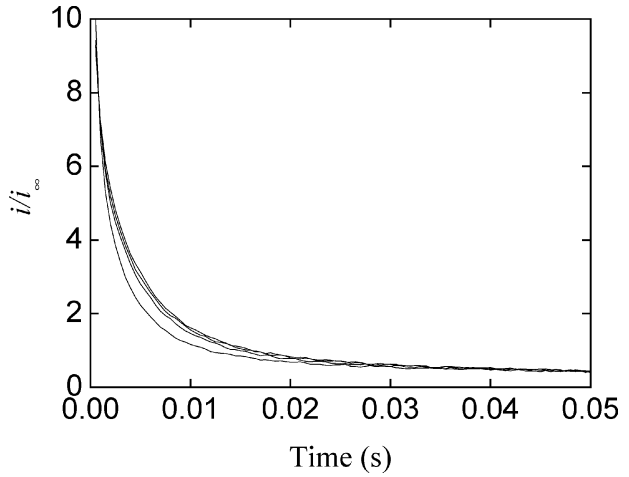


**Fig. 13** Measured normalised current–time response for the anodic dissolution of an Ag UME under potential step control, with the UME positioned 3 μm from the following interfaces: clean W/A interface (bottom line); and a W/A interface with a phospholipid monolayer at surface pressures of (from bottom to top) 10 mN $m^{-1}$, 20 mN $m^{-1}$, and 30 mN $m^{-1}$.

have been fitted to the two models: (a) the simple (potential-independent) adsorption process; and (b) a potential-dependent adsorption process.

The differences between the three series of measurements are quite clear when the data are presented in the form of Fig. 14, allowing us to obtain quantitative data of the uptake of $Ag^+$ ions by the monolayer. To fit the experimental values with the numerical simulations a fixed distance of 3.0 μm was set, as estimated by the hindered diffusion theory at the clean W/A interface. Given that both the rate constant and concentration of binding sites are variables, in fitting the data, we set a restriction that the value of the kinetic rate constant should be used for the three cases and changed the value of the concentration of binding sites. The fits shown in Fig. 14(a) for the simple potential-independent model, are for $K_a = 15$ (equivalent to $k_a = 0.18$ cm $s^{-1}$), which is just below—but distinguishable from—the diffusion limit. The fraction of binding sites obtained from the model was $\phi = 0.055$, $\phi = 0.068$, and $\phi = 0.082$, for surface pressures of 10 mN $m^{-1}$, 20 mN $m^{-1}$, and 30 mN $m^{-1}$. Taking into account the change in area per molecule with surface pressure, this corresponds to a reasonably constant percentage of deprotonated phospholipids of 20 ± 2 %, respectively, under the assumption of a simple (potential-independent) adsorption process. When a potential-dependent adsorption process is considered (Fig. 14(b)), the value of the intrinsic rate constant is estimated as $K_a^i = 5$ (equivalent to $k_a^i = 0.06$ cm $s^{-1}$), with the same values of the surface density of adsorption sites as in the potential-independent case. Note that there is very little difference in the goodness of fits for a potential-independent and potential-dependent models due to the low fixed charge concentration at the monolayer.

## Conclusions

SECM chronoamperometry has proven an effective technique for the measurement of silver ion adsorption kinetics at interfaces, illustrated through studies of $Ag^+$ binding to a DPPA Langmuir monolayer. The technique relies on the reversibility of the $Ag/Ag^+$ redox couple; the current for $Ag^+$ electrogeneration at an Ag UME is sensitive to the diffusive flux of $Ag^+$ away from the electrode surface which, in turn, is affected by any interaction of $Ag^+$ with a nearby interface. For $Ag^+$ binding to DPPA, the binding capacity of the monolayer was found to increase with surface pressure, which served to increase the density of adsorption sites. The adsorption process was described reasonably well as an irreversible process, with a

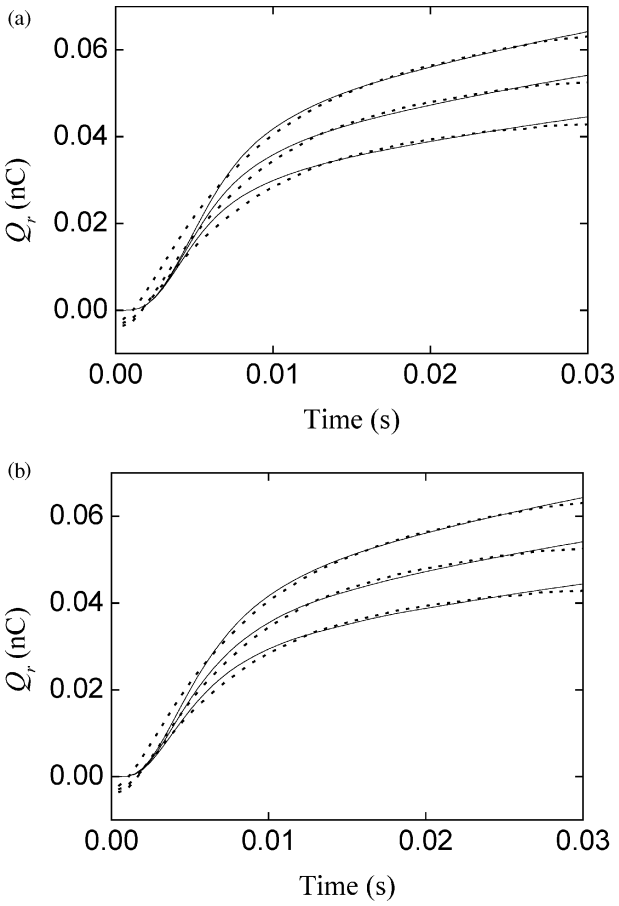


**Fig. 14** Experimental charge difference, $Q_r$ (dotted lines) as a function of time for a DPPA monolayer at surface pressures of (from bottom to top) 10 mN $m^{-1}$, 20 mN $m^{-1}$, and 30 mN $m^{-1}$. The best theoretical fits (solid lines) were obtained as outlined in the text considering either a simple (potential-independent) adsorption process (a) or a potential-dependent adsorption process (b).

rate constant of 0.18 cm $s^{-1}$, which was just distinguishable from the diffusion-controlled case.

There is scope for using this type of approach to study other adsorption and binding processes, where the adsorbate ion (or molecule) can be made part of a reversible electrode process. For example, it might be possible to use the stripping of heavy metal ions from mercury electrodes to study their interaction with interfaces. Building on preliminary work on $Ag^+$ ion adsorption and Ag metal deposition on pyrite,[55] we shall report further, in due course, on the use of this approach to study the kinetics of metal particle formation at several types of interfaces.

## Appendix

In electrochemical reactions, the evaluation of the surface concentrations to be used in the kinetic equations needs to take into account electrical double layer effects; this is known as the Frumkin correction. When the reaction surface is uniformly charged, the surface potential (*i.e.*, the potential drop in the electrical double layer) can be evaluated from the Gouy–Chapman theory. However, when using the SECM to study heterogeneous kinetics, it is found in several systems (*e.g.*, in the protonation of phospholipid monolayers[46] or in redox processes in metallopolymer thin films[56]) that the surface charge density is non-uniform. This means that the electric field is no longer just normal to the surface; it also has a component parallel to the surface. Moreover, the effect of the electrical double layer on the surface concentration can no longer be easily evaluated because the relation between the local surface

 

charge density and the local surface potential is unknown. Since a correct procedure to deal with this problem is lacking (or too complicated), it is often accepted that the Gouy–Chapman equation can still be used to relate the local surface charge density and the local surface potential, even though they vary along the surface and the Gouy–Chapman equation is strictly valid only for uniformly charged surfaces.[37] To the best of our knowledge, sound arguments that support the validity of this procedure have not been discussed in the literature and, therefore, we find it convenient to provide a validity criterion. Since we have in mind its application to SECM studies, this is done for a system with cylindrical symmetry.

The Poisson–Boltzmann equation in the solution adjacent to the reaction surface in the case of a 1 : 1 supporting electrolyte is

$$\frac{1}{r}\frac{\partial}{\partial r}\left(r\frac{\partial \varphi}{\partial r}\right)+\frac{\partial^2 \varphi}{\partial x^2}=\kappa^2 \sinh \varphi \qquad \text{(A1)}$$

where $r$ is the radial distance to the microelectrode axis, $x$ is the distance to the reaction surface, $\varphi \equiv F\psi/RT$ is the electric potential in $RT/F$ units, $\kappa \equiv [2F^2I/\varepsilon\varepsilon_0 RT]^{1/2}$ is the Debye parameter, and $I$ is the supporting electrolyte molar concentration. The boundary condition at the reaction surface is

$$\left.\frac{\partial \varphi}{\partial x}\right|_{x=0}=-\frac{F}{\varepsilon\varepsilon_0 RT}\sigma(r) \qquad \text{(A2)}$$

where $\sigma(r)$ is the surface charge density, which depends on the radial position.

If the surface charge density was uniform, the solution to this electrostatic problem leads to the Gouy–Chapman equation

$$\varphi^s \equiv \varphi(x=0)=2\,\mathrm{arcsin\,h}\frac{\sigma F}{2\varepsilon\varepsilon_0\kappa RT}. \qquad \text{(A3)}$$

When the surface charge density is non-uniform, the radial gradient of the electric potential at the reaction surface can be approximately estimated as

$$\left.\frac{\partial \varphi}{\partial r}\right|_{x=0}\approx\frac{\mathrm{d}\varphi^{\mathrm{s}}}{\mathrm{d}r}=2\frac{\mathrm{d}\sigma}{\mathrm{d}r}\frac{\mathrm{d}}{\mathrm{d}\sigma}\left[\mathrm{arcsin\,h}\frac{\sigma F}{2\varepsilon\varepsilon_0\kappa RT}\right]$$
$$=-\frac{\mathrm{d}\sigma}{\mathrm{d}r}\frac{F}{\varepsilon\varepsilon_0\kappa RT}\frac{1}{\cosh(\varphi^{\mathrm{s}}/2)}. \qquad \text{(A4)}$$

The Gouy–Chapman equation is expected to be approximately valid (for non-uniformly charged surfaces) when this radial gradient is much smaller (in magnitude) than the axial gradient given by eqn. (A2), that is, when

$$\left|\frac{\mathrm{d}\sigma}{\mathrm{d}r}\right| \ll \left|\frac{\sigma}{\kappa}\right| \qquad \text{(A5)}$$

for cases where $\cosh(\varphi^{\mathrm{s}}/2) \geq 1$. Eqn. (A5) means that the length scale for the radial variation of the surface charge density must be larger than the Debye length in solution (*i.e.* the reciprocal of the Debye parameter).

The mathematical consistency of this derivation requires that the first term in the left hand side of eqn. (A1), when approximately evaluated as $(1/r)\mathrm{d}(r\mathrm{d}\varphi^{\mathrm{s}}/\mathrm{d}r)/\mathrm{d}r$, must be much smaller than the right hand side of this equation. This has been checked numerically for some functions $\sigma(r)$ and found to be satisfied when eqn. (A5) is fulfilled.

## Acknowledgements

D. P. B. and D. M. gratefully acknowledge the EPSRC for funding. We appreciate support from the EU Human Potential Program SUSANA (Supramolecular Self-Assembly of Interfacial Nanostructures). J. V. M. thanks the Royal Society for the award of a University Research Fellowship.

## References

1 B. Volesky and Z. R. Holan, *Biotechnol. Prog.*, 1995, **11**, 235.
2 E. J. Harris, in *Transport and Accumulation in Biological Systems*, ed. E. J. Harris, Butterworth & Co Publishers, Ltd., London, University Park Press, Baltimore, 1972, pp. 109–110.
3 Z. Reddad, C. Gerente, Y. Andres and P. Le Cloirec, *Environ. Sci. Technol.*, 2002, **36**, 2067.
4 N. Goyal, S. C. Jain and U. C. Banerjee, *Adv. Environ. Res.*, 2003, **7**, 311.
5 B. Greene, M. Hosea, R. McPherson, M. Henzi, M. D. Alexander and D. W. Darnall, *Environ. Sci. Technol.*, 1986, **20**, 627.
6 C. A. Mahan and J. A. Holcombe, *Anal. Chem.*, 1992, **64**, 1933.
7 W. W. Kubiak, J. Wang and D. Darnall, *Anal. Chem.*, 1989**61**, 468.
8 M. K. Jain, *The Bimolecular Lipid Membrane*, Van Nostrand Reinhold Company, New York, 1972, pp. 179–180.
9 T. Skowroński, *Chemosphere*, 1984, **13**, 1385.
10 H.-Y. D. Ke, E. R. Birnbaum, D. W. Darnall, G. D. Rayson and P. J. Jackson, *Environ. Sci. Technol.*, 1992, **26**, 782.
11 H.-Y. D. Ke, W. L. Anderson, R. M. Moncrief, G. D. Rayson and P. J. Jackson, *Environ. Sci. Technol.*, 1994, **28**, 586.
12 V. Majidi, D. A. Laude, Jr. and J. A. Holcombe, *Environ. Sci. Technol.*, 1990, **24**, 1309.
13 L. R. Drake, S. Lin, G. D. Rayson and P. J. Jackson, *Environ. Sci. Technol.*, 1996, **30**, 110.
14 J. L. Gardea-Torresdey, M. K. Becker-Hapak, J. M. Hosea and D. W. Darnell, *Environ. Sci. Technol.*, 1990, **24**, 1372.
15 M. C. Phillips and D. Chapman, *Biochim. Biophys. Acta*, 1968, **163**, 301.
16 R. C. MacDonald and S. A. Simon, *Proc. Natl. Acad. Sci. USA*, 1987, **84**, 4089.
17 D. Marsh, *Biochim. Biophys. Acta*, 1996, **1286**, 183.
18 H. Brockman, *Curr. Opin. Struct. Biol.*, 1999, **9**, 438.
19 F. Sun, *Biophys. J.*, 2002, **82**, 2511.
20 M. Yazdanian, H. Yu and G. Zografi, *Langmuir*, 1992, **8**, 630.
21 T. Y. Kim and D. J. Ahn, *Mater. Sci. Eng, C.*, 2004, **24**, 205.
22 J. Y. Hyun, G. S. Lee, T. Y. Kim and D. J. Ahn, *Korean J. Chem. Eng.*, 1997, **14**, 533.
23 W. Zhao, M. Won Kim, D. B. Wurm, S. T. Brittain and Y.-T. Kim, *Langmuir*, 1996, **12**, 386.
24 L. M. Eng, C. Seuret, H. Looser and P. Günter, *J. Vac. Sci. Technol. B*, 1996, **14**, 1386.
25 J. G. Petrov, I. Kuleff and D. Platikanov, *J. Colloid Interface Sci.*, 1982, **88**, 29.
26 J. Heinze, *Angew. Chem., Int. Ed. Engl.*, 1993, **32**, 1268.
27 R. J. Forster, *Chem. Soc. Rev.*, 1994, 289.
28 R. J. Forster, in *Encyclopedia of Electrochemistry*, ed. A. J. Bard, M. Stratmann and P. R. Unwin, Wiley-VCH, Weinheim, Germany, 2003, vol. 3, pp. 160–195.
29 R. M. Wightman, *Science*, 1988, **240**, 415.
30 R. M. Wightman and D. O. Wipf, *Acc. Chem. Res.*, 1990, **23**, 64.
31 A. J. Bard and M. V. Mirkin, in *Scanning Electrochemical Microscopy*, ed. A. J. Bard and M. V. Mirkin, Marcel Dekker, New York, 2001.
32 A. J. Bard, F.-R. F. Fan, D. T. Pierce, P. R. Unwin, D. O. Wipf and F. Zhou, *Science*, 1991, **254**, 68.
33 A. L. Barker, M. Gonsalves, J. V. Macpherson, C. J. Slevin and P. R. Unwin, *Anal. Chim. Acta*, 1999, **385**, 223.
34 A. L. Barker, C. J. Slevin, P. R. Unwin and J. Zhang, in *Liquid Interfaces in Chemical, Biological, and Pharmaceutical Applications*, ed. A. G. Voltov, Marcel Dekker, New York, 2001.
35 M. V. Mirkin, *Anal. Chem.*, 1996, **68**, 177A.
36 A. L. Barker, C. E. Gardner, J. V. Macpherson, P. R. Unwin and J. Zhang, in *Biomolecular Films: Design, Function and Applications*, ed. J. F. Rusling, Marcel Dekker, New York, USA, 2003, pp. 253–335.
37 P. R. Unwin and A. J. Bard, *J. Phys. Chem.*, 1992, **96**, 5035.
38 C. J. Slevin and P. R. Unwin, *J. Am. Chem. Soc.*, 2000, **122**, 2597.
39 C. J. Slevin, P. Liljeroth and K. Kontturi, *Langmuir*, 2003, **19**, 2851.
40 C. J. Slevin, S. Ryley, D. J. Walton and P. R. Unwin, *Langmuir*, 1998, **14**, 5331.
41 I. Ciani, D. P. Burt, S. Daniele and P. R. Unwin, *J. Phys. Chem. B*, 2004, **108**, 3801.
42 S. Cannan, J. Zhang, F. Grunfeld and P. R. Unwin, *Langmuir*, 2004, **20**, 701.
43 J. Zhang and P. R. Unwin, *Langmuir*, 2002, **18**, 1218.
44 J. Zhang and P. R. Unwin, *Phys. Chem. Chem. Phys.*, 2003, **5**, 3979.
45 J. Zhang, C. J. Slevin, C. Morton, P. Scott, D. J. Walton and P. R. Unwin, *J. Phys. Chem. B*, 2001, **105**, 11120.
46 J. Zhang and P. R. Unwin, *J. Am. Chem. Soc.*, 2002, **124**, 2379.

47 J. Zhang and P. R. Unwin, *Phys. Chem. Chem. Phys.*, 2002, **4**, 3814.
48 P. R. Unwin, *J. Chem. Soc., Faraday Trans.*, 1998, **94**, 3183.
49 A. J. Bard and L. R. Faulkner, *Electrochemical Methods: Fundamentals and Applications*, John Wiley & Sons, New York, 2001.
50 C. J. Slevin, J. A. Umbers, J. H. Atherton and P. R. Unwin, *J. Chem. Soc., Faraday Trans.*, 1996, **92**, 5177.
51 J. Kwak and A. J. Bard, *Anal. Chem.*, 1989, **61**, 1221.
52 D. Pletcher and S. J. Sotiropoulos, *J. Chem. Soc., Faraday Trans.*, 1995, **91**, 457.
53 J. Minones, J. M. Rodriguez Patino, J. Minones, P. Dynarowicz-Latka and C. Carrera, *J. Colloid Interface Sci.*, 2002, **249**, 388.
54 K. de Meijere, G. Brezesinski, K. Kjaer and H. Möhwald, *Langmuir*, 1998, **14**, 4204.
55 P. R. Unwin, J. V. Macpherson, R. D. Martin and C. F. McConville, *Proc. Electrochem. Soc.*, 2000, **99–28**, 104.
56 A. P. O'Mullane, J. V. Macpherson, P. R. Unwin, J. Cervera-Montesinos, J. A. Manzanares, F. Frehill and J. G. Vos, *J. Phys. Chem. B*, 2004, **108**, 7219.

 